Drag Reduction via Large-scale Opposition Flow Control in a High-Reynolds-number Turbulent Boundary Layer

M. R. Abbassi, W. J. Baars, N. Hutchins and I. Marusic

Department of Mechanical Engineering, The University of Melbourne, Parkville, VIC 3010, Australia

Abstract

Studies over the past decade have shown that large-scale coherent structures (superstructures) in the logarithmic region of a high-Reynolds-number turbulent boundary layer play an important role in the dynamics of the near-wall turbulence. Consequently, it is hypothesized that the skin-friction drag can potentially be reduced using a flow control scheme that targets the large-scale structures. Here we employ a large-scale blowing-only opposition flow control scheme in an attempt to reduce the turbulence intensity of the large-scales and to deduce how that affects the mean wall-shear stress. The study was conducted in a turbulent boundary layer at a friction Reynolds number of $Re_\tau \approx 14\,790$. Wall-normal jet flows were used as actuators to manipulate the structures affiliated with positive wall-shear stress signatures. A reduction of 8% is observed in the pre-multiplied power spectral density of the large-scale streamwise velocity fluctuations in the logarithmic region. Additionally, the small-scale streamwise fluctuating energy is enhanced by 5% in the logarithmic region suggesting that the jets have introduced additional small scale turbulence into the logarithmic region. A maximum skin-friction drag reduction of 3.5% was achieved at 1.6δ downstream of the actuators, evaluated via hot-film shear-stress sensors. The relative amplitudes of both the high- and low-speed events have been reduced, which is believed to be a result of the abated counter-rotating roll modes that are affiliated with these events.

Introduction

Superstructures in the regions above the near-wall cycle, have been shown to become increasingly energetic with higher Reynolds numbers. The turbulent activities associated with these structures become comparable to those of the small-scale structures in the near-wall region [6] and their presence leave a distinct imprint in the near-wall cycle, and, on the wall as large-scale skin-friction fluctuations [1, 5, 9]. Indeed, large-scale flow control of this type has previously been developed by Schoppa and Hussain [11] in DNS simulations. It is conjectured that manipulating the large-scale coherent structures in the logarithmic region of a high-Reynolds-number turbulent boundary layer has the potential to result in reduction of the mean wall-shear stress due to elimination of the instantaneous positive wall-shear stress fluctuations. Large-scale structures can be categorized as large regions of streamwise velocity deficit on the order of the boundary layer thickness δ, flanked on both sides in the spanwise direction by large regions of velocity surplus. Hereafter, the former and the latter structures are referred to as low- and high-speed events, respectively. These large-scale regions are accompanied by large-scale counter-rotating roll modes [6], the up- and down-wash sides of which accompany the low- and high-speed events, respectively [9, 3, 4].

The present study is aimed at an active flow control scheme which operates in real-time in order to manipulate the large-scale coherent structures residing in regions above the near-wall cycle in an opposition framework. To that effect, we utilized wall-normal jet flows as actuators which were triggered by upstream wall-based sensors. The best candidates of the large-scale structures to be counteracted by the applied jet airflows in an opposition scenario have been chosen to be the down-wash sides of the roll modes, which were detected implicitly by sensing the footprints of the high-speed events on the wall. In an earlier study, [10] showed the feasibility of the control scheme that is going to be implemented here. They used only one wall-normal jet actuator, while we extend the number of actuators to nine and distribute them in the spanwise direction in order to accommodate the width of the large-scale structures and additionally account for the meandering feature of such structures.

Experimental Set-up

The Experimental Facility and Conditions

The experiments were conducted in the High Reynolds Number Boundary Layer Wind Tunnel (HRNBLWT) at the University of Melbourne [2]. For the conditions we consider in this paper, the friction velocity of the measurement is $U_{\tau_u} = 0.641$ ms^{-1}, which with a boundary layer thickness of $\delta = 0.368$m at the measuring section provides a friction Reynolds-number of $Re_\tau = U_{\tau_u}\delta/\nu \approx 14\,790$. The chosen coordinate system is shown in figure 1.

The Control Components

The large-scale wall-shear stress fluctuations were measured via nine Dantec glue-on probes (55R47)—shown in figure 1—as surrogates for detecting the large-scale structures in the logarithmic region. The spanwise spacings of the hot-films were adopted from [7] to be 26mm ($0.08\delta \sim 1060$ wall units). The whole spanwise array of hot-films accommodate approximately twice the width of the detected footprint of the structures. In order for the hot-film signals to represent the passage of the large-scale structures, time-series were filtered using convolution of a 1.5δ-long Gaussian filter (Taylor's hypothesis with a convection velocity of 13.92 ms^{-1} was used to convert space to time). The positive values of the filtered signals are then interpreted as the footprints of the passage of the high-speed events, whereas the negative values are accordingly interpreted as the footprints of the passage of the low-speed events. The positive and negative values are converted to a respective *high* and *low* voltage levels of a transistor-transistor logic (TTL) digital control signal.

Nine streamwise jet slots—each with a jet exit plane of 50mm × 2mm (2038 × 82 wall units)—were flush mounted downstream of the sensors and aligned with them in the spanwise direction, in order to introduce wall-normal jet flows into the boundary layer—shown in figure 1. The output pressure of the pressure regulator connected to the jet slots is set such that an exit velocity of 12.93 ms^{-1} ($\approx 0.65U_\infty$) at the centroid of the jet exit plane is provided in still air.

In practical applications there is a finite time delay between the detection and the actuation, which for the current control
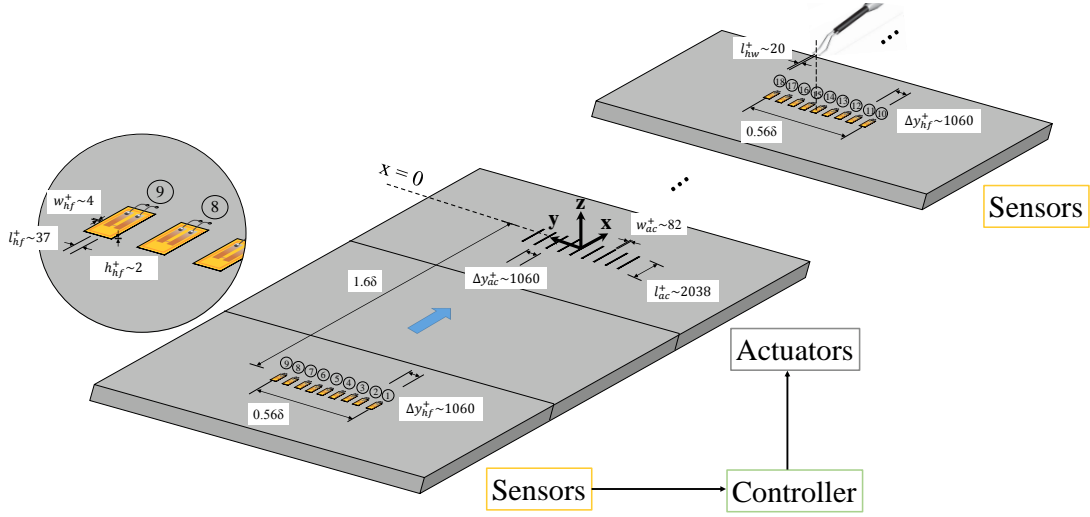
Figure 1: Schematic representation of the sensors and actuators with their respective dimensions and spacings.

set-up is a function of three parameters: the delay between the *high* value of the TTL control signal and the airflow from the jet exit plane (≈ 14.3ms), the delay due to the Task Execution Time of the controller (TET ≈ 0.2ms) and the delay due to the time shift of the impulse response of the Gaussian filter, since the filter is ought to be implemented in real-time (≈ 20.5ms). Summing up all these individual delays results in an overall time delay of 35.1ms, during which the structures have already reached 0.48m downstream of the detection location.

Furthermore, due to the slight inclination of the large-scale coherent structures to the horizontal, the actuators need to be triggered prior to the arrival of the detected footprint of the superstructures at the location of the actuators. This advance in time is a function of the inclination angle of the structures, which in turn is a function of the size of the structures and their corresponding wall-normal heights. The current control scheme is synchronized in such a way that by the time the streamwise location of the large-scale structures (i.e. those structures with a wavelength greater than 1.5δ) that reside in the geometric centre of the logarithmic region is predicted to convect above the streamwise location of the actuators, the compressed airflow has reached the jet exit planes of the actuators. In order to accommodate the temporal precedence of actuation due to the inclination of the structures, the actuators are moved 0.12m further downstream, resulting in a streamwise spacing of 0.6m ($\sim 1.6\delta$)—the spacial information is determined by using a convection velocity of 13.92ms^{-1}.

The Measurement Techniques

A boundary layer survey was performed within the range $0.35 < z < 525$mm, with 40 logarithmically spaced wall-normal heights. The results presented for wall-shear stress fluctuations are measured via hot-film sensors similar to those sensors that have been used for structure detection—shown in figure 1. The calibration procedure for the measuring hot-films has been carried out *in situ* against unit Reynolds-number (U_∞/ν), which had been precalibrated against the wall-shear stress (τ_w) using a floating-element skin-friction sensor [2], that provided wall-shear stress information for the same downstream location as that of the hot-films.

Experimental Results and Discussion

Streamwise Evolution of Control in the Logarithmic Region

The variations of the velocity fluctuations due to the control scheme has been measured in the streamwise direction at a single wall-normal height ($z^+ \approx 477$), which corresponds to that of the outer-peak in the pre-multiplied spectrum [8]

($z^+ \approx 3.9Re_\tau^{1/2}$). The variations in the mean velocity and turbulence intensity have been shown in figure 2(a), in terms of percentage. The corresponding change in the energy spectrum is plotted in 2(b).
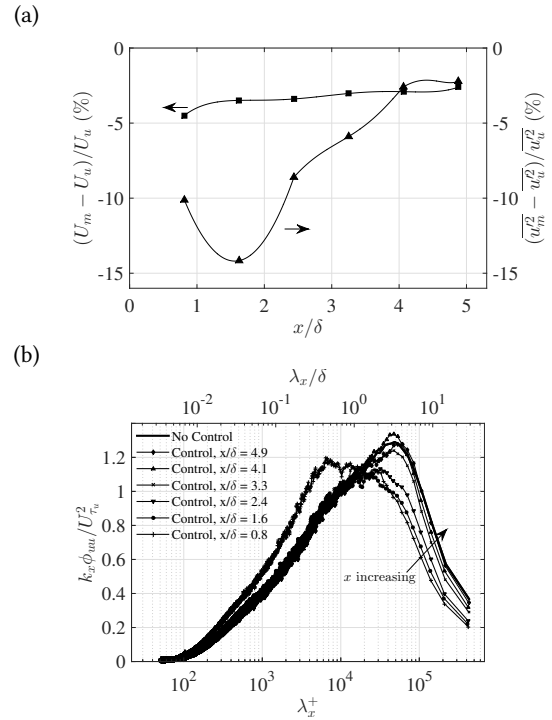
(a)

(b)

Figure 2: (a) Square: percentage variation of the mean streamwise velocity; triangle: percentage variation of the turbulence intensity. (b) Pre-multiplied energy spectrum downstream of the actuators. *u* and *m* stand for unmanipulated and manipulated flows, respectively. The measurements have been conducted at a wall-normal height of $z^+ \approx 477$.

As figure 2(a) suggests, the mean streamwise velocity has been reduced, which is due to the fact that wall-normal jet flows do not possess any streamwise momentum. This results in a mean streamwise velocity of the manipulated turbulent boundary layer which is lower than that of the unmanipulated case. The percentage variation of the turbulence intensity demonstrates a maximum reduction at 1.6δ downstream of the actuators. Both the velocity deficit and the reduction in the turbulence intensity recover as one moves further downstream of the actuators.

According to figure 2(b), the measurement point at $x = 0.8\delta$ demonstrates an increase in the energy associated to the small-scale structures (i.e. $\lambda_x < 1.5\delta$) together with a decrease in the energy of the large-scale structures (i.e. $\lambda_x > 1.5\delta$). The observed increase of the energy of the small-scale structures can be associated to the lift of these structures away from the wall via the wall-normal jet airflows, which descend very quickly onto the wall—as inferred from the collapse of the energy associated to $\lambda_x < 1.5\delta$ to that of the unmanipulated energy distribution. However, the decrease in the pre-multiplied energy spectra of the large-scale structures persists for a much larger streamwise distance and gradually converges towards the unmanipulated spectrum by moving further downstream from the actuators.

Control Effect on Energy Spectra

In order to distinguish the pre-multiplied energy spectrum of the controlled boundary layer from that of the unmanipulated one, the difference in the spectra, $\Delta k_x \Phi_{uu}/U_{\tau_u}^2 = k_x(\Phi_{u_m u_m} - \Phi_{u_u u_u})/U_{\tau_u}^2$, accompanied by two levels of the spectra contour of the unmanipulated flow: 1.1 and 1.3, has been plotted in figure 3. The lower- and upper-bound of the logarithmic region as well as the scale-separating wavelength ($\lambda_x^+ \approx 7000$, [6]) have also been marked in figure 3. As such, the wall-normal–wavelength domain ($z^+ - \lambda_x^+$) is divided into 6 discernible regions, which are denoted by I-VI in figure 3.

According to figure 3, the majority of the energy reduction occurs in regions associated to the large-scale structures (i.e. within the regions IV, V and VI), which warrants the fact that the implemented control scheme has been successful in languishing the large-scale structures in the turbulent boundary layer and most importantly those energetic structures which populate the logarithmic region. For the purpose of the current study, the behavioural changes of regions IV and V are mainly of interest, since they are associated to the large-scale coherent structures in the near-wall and the logarithmic regions of the boundary layer, respectively.
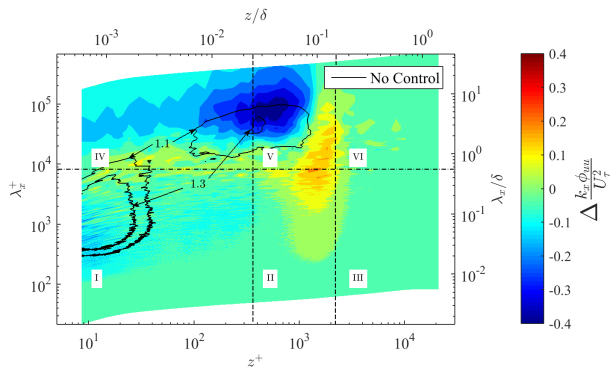

Figure 3: Iso-contours of $\Delta k_x \Phi_{uu}/U_{\tau_u}^2 = k_x(\Phi_{u_m u_m} - \Phi_{u_u u_u})/U_{\tau_u}^2$, with three contour levels of $k_x \Phi_{u_u u_u}/U_\tau^2$. u and m stand for unmanipulated and manipulated flows, respectively. Boundary layer measurements at 1.6δ downstream of the actuators.

The total energy of region V has been reduced by 8.0%. However, there is a local increase in the energy at the lower-right section of region V and upper-right section of region II in figure 3, which is due to the imprint of the upper part of the wall-normal jet airflow into the boundary layer, resulting in an energy increase of 5% in region II. According to region IV of figure 3, the energy reduction of the large-scale structures has been cascaded from the logarithmic region towards the wall.

Control Effect on Conditional Events

The streamwise velocity fluctuations are plotted in a conditional sense, whose procedure can be summarized in the following formula: $\tilde{u}^+(x + 1.6\delta, 0, z) = \langle u(x + 1.6\delta, 0, z)|u_\tau(x - 1.6\delta, 0, 0) = 0$ & $\partial_x u_\tau(x - 1.6\delta, 0, 0) < 0\rangle/U_{\tau_u}$. The results of such conditional averages for the unmanipulated and the controlled boundary layers are plotted in figures 4(a) and (b), respectively. The condition is chosen to be the change in the sign of the signal of hot-film number 5 from minus to positive, which indicates a transition of the footprint of a low-speed event to that of a high-speed event.
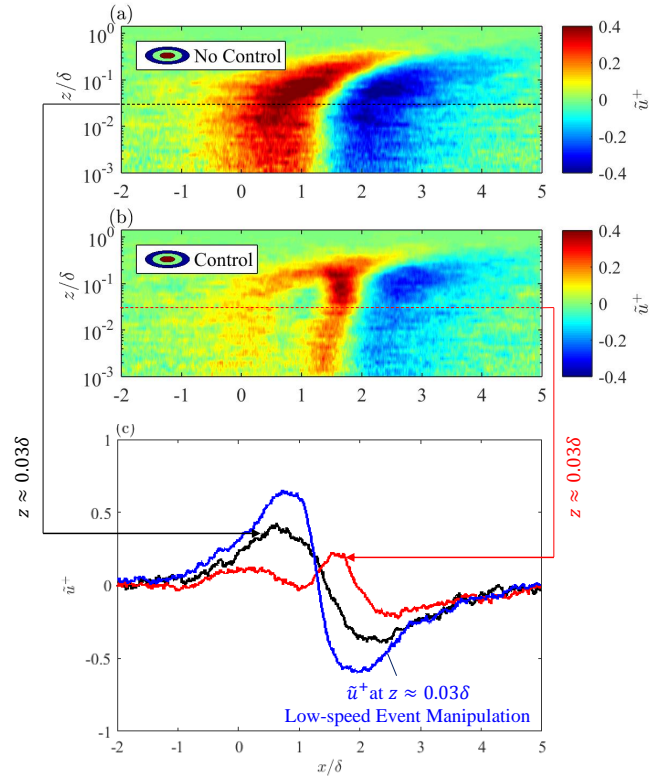

Figure 4: Conditionally averaged streamwise velocity fluctuations. Iso-contours of the two-dimensional view of the streamwise–wall-normal plane for the unmanipulated boundary layer, (a); and the controlled boundary layer, (b). (c) One-dimensional view in the streamwise direction for the unmanipulated and the controlled boundary layers at $z \approx 0.03\delta$, accompanied by the corresponding conditional average for the low-speed event manipulation case, which is denoted on the figure.

The conditional average for the case when the wall-normal jet actuators were triggered by the low-speed events has also been plotted figure 4(c). The result of such manipulation has been presented only for a single wall-normal height of $z^+ \approx 477 (\sim 0.03\delta)$, together with its counterparts of the unmanipulated and the high-speed event manipulation cases. According to figure 4(c) it can be concluded that as the wall-normal jet airflows act upon the large-scale high-speed events, it results in the deceleration of the high-speed events and acceleration of the low-speed events, which is a manifestation of the weakening of the accompanying counter-rotating roll modes. The opposite phenomenon occurs if the actuation is upon the low-speed events. For the case of the random manipulation it is speculated that on average the wall-normal jet airflows target half of the high-speed events whereas the other half of manipulation is upon the low-speed events. As such, the detrimental effect of the low-speed event manipulation counteracts the beneficial effect of the high-speed event manipulation and ultimately the net effect would be the same as the unmanipulated

turbulent boundary layer.

Control Effect on Wall-shear Stress

The hot-film sensors are highly susceptible to the change in the temperature of the substrate to such extend that during the course of the measurement, they might occasionally exceed beyond or fall below the range of their respective calibration curves. And this is due to fact that they are directly affixed on the wall. If such substantial drift was observed in the hot-film signals, they were discarded in the post processing stage. The only hot-film among all the downstream measuring hot-films which fulfils such criterion is hot-film number 11 and here we only report the results of that hot-film.

The probability density function (PDF) of the large-scale skin-friction fluctuations is shown in figure 5 for both the uncontrolled and controlled turbulent boundary layer at $x = 1.6\delta, y = -0.21\delta$, corresponding to the position of hot-film number 11. The reason why only the large-scale components of the wall-shear stress fluctuations have been presented is due to the fact that the hot-film sensors are not capable of resolving the high frequency fluctuations accurately. As shown in figure 5, the PDF distributions for both the uncontrolled and the controlled cases resemble normal distributions. The mean value of the signal of which a normal distribution represents, is equal to the value corresponding to the peak of that distribution. Therefore, the reduction of the mean of the wall-shear stress fluctuations due to the control scheme is clearly visible in figure 5 and is calculated to be 3.5%. The corresponding percentage reduction of the respective variance is 18.75%.
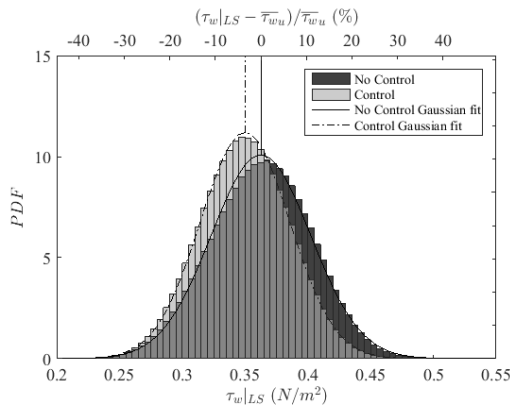

Figure 5: Probability density function of the large-scale wall-shear stress fluctuations ($\tau_w|_{LS}$) at $x = 1.6\delta, y = -0.21\delta$ for the uncontrolled (dark histogram) and the controlled (light histogram) flows. The percentage variation with respect to the unmanipulated mean wall-shear stress has been shown on the top axis. The respective Gaussian fit distributions are also shown.

The above-mentioned measured skin-friction reduction is the most important and positive outcome arising from the results, which confirms the premise that has been hypothesized in the introduction. In other words, skin-friction drag reduction can indeed be obtained by a large-scale opposition flow control in a high-Reynolds-number turbulent boundary layer. To the knowledge of the authors this is the first time that a large-scale control scheme has been implemented experimentally and its success has been shown evidently.

Furthermore, we speculate that the drag reduction at the centreline of the array of the measuring hot-film sensors (i.e. $x = 1.6\delta, y = 0$) might be even larger that shown in 5, since the manipulated wall variables at $x = 1.6\delta, y = 0$ with respect to those at $x = 1.6\delta, y = -0.21\delta$ might not be affected by the recovering

edge of the control zone.

Conclusion

A large-scale blowing-only opposition flow control scheme has been implemented to a high-Reynolds-number turbulent boundary layer. 3.5% skin-friction drag reduction has been shown to be accomplished by reducing the energy of the large-scale coherent structures in the logarithmic region of a high-Reynolds-number turbulent boundary layer.

Acknowledgements

References

[1] Abe, H., Kawamura, H. and Choi, H., Very Large-Scale Structures and their Effects on the Wall Shear-Stress Fluctuations in a Turbulent Channel Flow up to Re_τ=640, *J. Fluids Eng.*, **126**, 2004, 835–843.

[2] Baars, W. J., Squire, D. T., Talluru, K. M., Abbassi, M. R., Hutchins, N. and Marusic, I., Wall-Drag Measurements of Smooth- and Rough-Wall Turbulent Boundary Layers Using a Floating Element, *Exp. Fluids*, **57**, 2016, 1–16.

[3] Dennis, D. J. C. and Nickels, T. B., Experimental Measurement of Large-Scale Three-Dimensional Structures in a Turbulent Boundary Layer. Part 1. Vortex Packets, *J. Fluid Mech.*, **673**, 2011, 180–217.

[4] Hutchins, N., Chauhan, K., Marusic, I., Monty, J. and Klewicki, J., Towards Reconciling the Large-Scale Structure of Turbulent Boundary Layers in the Atmosphere and Laboratory, *Bound-Lay. Meteorol.*, **145**, 2012, 273–306.

[5] Hutchins, N. and Marusic, I., Evidence of Very Long Meandering Features in the Logarithmic Region of Turbulent Boundary Layers, *J. Fluid Mech.*, **579**, 2007, 1–28.

[6] Hutchins, N. and Marusic, I., Large-Scale Influences in Near-Wall Turbulence, *Phil. Trans. R. Soc. A*, **365**, 2007, 647–664.

[7] Hutchins, N., Monty, J. P., Ganapathisubramani, B., Ng, H. C. H. and Marusic, I., Three-Dimensional Conditional Structure of a High-Reynolds-Number Turbulent Boundary Layer, *J. Fluid Mech.*, **673**, 2011, 255–285.

[8] Marusic, I., Mathis, R. and Hutchins, N., High Reynolds Number Effects in Wall Turbulence, *Int. J. Heat Fluid Fl.*, **31**, 2010, 418–428.

[9] Marusic, I., Mathis, R. and Hutchins, N., Predictive Model for Wall-Bounded Turbulent Flow, *Science*, **329**, 2010, 193–196.

[10] Marusic, I., Talluru, K. M. and Hutchins, N., Controlling the Large-scale Motions in a Turbulent Boundary Layer, in *Fluid-Structure-Sound Interactions and Control*, Springer, 2014, 17–26.

[11] Schoppa, W. and Hussain, F., A Large-Scale Control Strategy for Drag Reduction in Turbulent Boundary Layers, *Phys. Fluids*, **10**, 1998, 1049–1051.